JOURNAL OF MATERIALS SCIENCE 17 (1982) 1963–1976

Compressive fracture of polystyrene

D. KELLS*, N. J. MILLS
Department of Metallurgy and Materials, University of Birmingham, Birmingham, UK

Polystyrene cylinders and blocks were compressed with a variety of flat indentors until fracture occurred. The test cannot be interpreted solely by slip-line field theory, nor solely using Kendall's theory for the splitting of pre-cracked blocks of elastic material. A slip-line field analysis was made of the stress variation within the yielded zone beneath the indentor, then a boundary element analysis was made of the remaining cracked elastic region. This predicted stress intensity factors that are of the correct magnitude for the observed crack velocity.

1. Introduction

Diametral compression tests on polystyrene cylinders were carried out as part of an investigation of fracture processes that are initiated by yielding. Polystyrene is a convenient material to work with; its transparency allows crack growth to be observed and its photoelastic behaviour allows estimates to be made of elastic stress fields near yielded zones and cracks. The mechanical properties of polystyrene are well characterized; in tensile tests at room temperature it crazes, then cracks initiate and grow in the crazes [1], whereas in plane-strain compression tests polystyrene yields inhomogeneously, forming patterns of shear bands [2]. The diametral compression test, used as an indirect tensile test for concrete [3], is used here as a means of carrying out a plane-strain indentation test on a relatively small amount of material.

In the compression tests a limited amount of yielding occurs beneath the indentor, then a crack initiates at the tip of the yielded zone. The mechanics of crack initiation have been analysed in a previous paper [4], and here we concentrate on the crack-growth processes. To analyse the situation we need a form of elastic–plastic fracture mechanics, and in solving this problem we hope to aid the analysis of some of the many types of elastic–plastic fractures that occur in other materials and for other loading geometries. In a theoretical analysis we consider first a model that ignores crack propagation and then a model that ignores the yielded zone, in order to extract features that can be combined in a more complete analysis.

2. Stress analysis and yielding and crack growth beneath indentors

2.1. Simultaneous yield and fracture of a slab

Izbicki [5] analysed the partly-ductile fracture of a slab compressed between two indentors, using slip-line field methods. Because the material outside the yielded zone is assumed to be rigid (of infinite elastic modulus), it is necessary for the whole of the crack to form at once, so that the velocity field, or hodograph, is kinematically admissable. The approach will give an upper bound to the indentation pressure. Izbicki assumed that the material obeyed Griffith's failure criterion so that yielding occurs if

$$(\sigma_1 - \sigma_2)^2 + 8S_t(\sigma_1 + \sigma_2) = 0; \quad \text{for } 3\sigma_1 + \sigma_2 \leqslant 0, \tag{1}$$

and it suffers brittle fracture when

$$\sigma_1 = S_t; \text{for } 3\sigma_1 + \sigma_2 \geqslant 0, \tag{2}$$

where σ_1 and σ_2 are the principal stresses, with $\sigma_1 > \sigma_2$ and tensile stresses being positive, and S_t is the tensile strength of the material. Fig. 1 shows this failure criterion and Fig. 2a shows its application to indentation of a block of height $2h$ by

*Present address: Department of Non-metallic Materials, Brunel University, Uxbridge, UK.

0022–2461/82/071963–14$04.18/0

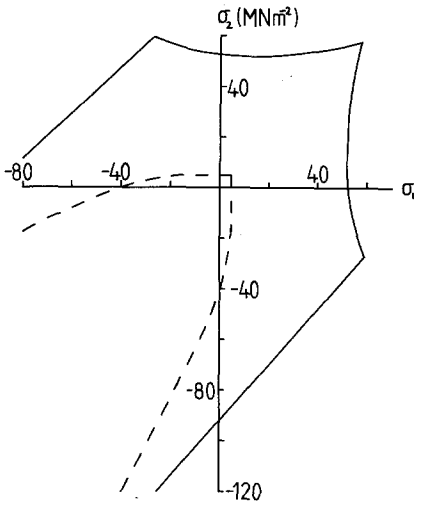

Figure 1 Plane-stress failure criterion: for polystyrene, Equations 5 and 6, solid line; and for concrete, Equations 1 and 2, with $S_t = 5$ MN m^{-2}, dashed line.

two rigid flat indentors of width $2w$. The slip-line field beneath the indentor was constructed by standard methods, but the important feature to notice is that it extends through the thickness of the block, so that the region to the left of DEF and to the right of CEF (in Fig. 2a) move away horizontally as the indentors penetrate the block.

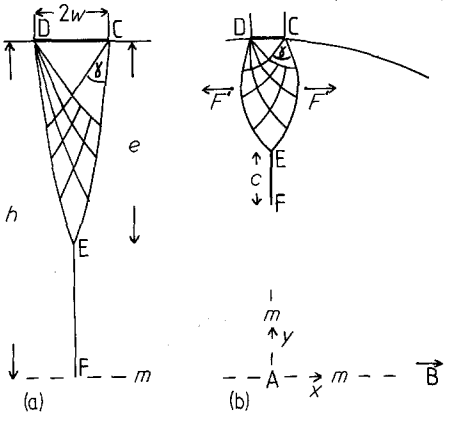

Figure 2 (a) Izbicki's slip-line field for the failure of a block of material obeying Equations 1 and 2, which occurs at an indentation pressure of 15 S_t when the block of half-thickness, h, is 8.96 times the indentor half-width, W, and m is a mirror symmetry line. (b) slip-line field for the plane strain indentation of a cylinder of polystyrene having the Coulomb yield criterion of Equation 5. The crack extends from E to the centre, A, for the complete slip-line field considered in Section 2.1., but only from E to F for the incomplete slip-line field used in Section 2.3. The pair of splitting forces, F', are used later to help match the experimental isochromatic fringe pattern.

Tensile fracture occurs under a stress $\sigma_{xx} = S_t$ along EF (in Fig. 2a), and shear failure occurs in the region CED (in Fig. 2a). The parameters in Fig. 2a are $h = 8.96w$, $e = 5.4w$ and $\gamma = 28°$. Chen [6] discusses the application of this result to the diametral compression of concrete, and shows that it gives a fracture load that is only 6.5% different from that calculated on the conventional elastic analysis. The latter states that the tensile stress, σ_{xx}, is

$$\sigma_{xx} = 2P/\pi D, \tag{3}$$

along the diameter AB of a cylinder of diameter, D, that is loaded by opposed-line loads at A and B of magnitude P per unit length.

The analysis of Izbicki can be adapted for polystyrene by inserting the appropriate yield and fracture criteria. In our previous paper [4] we assumed that polystyrene had a failure criterion that was a combination of Coulomb's yield criterion, and a critical strain criterion for crazing [7]. The Coulomb criterion can either be written in terms of τ and σ, the shear and normal stress components acting on the failure plane, as

$$|\tau| = \tau_0 - \sigma \tan \phi, \tag{4}$$

where the constants $\tau_0 = 46$ MN m^{-2} and $\phi = 5°$ for polystyrene, or in terms of the principal stresses as

$$\sigma_1 = \sigma_2 \tan^2(\pi/4 + \phi/2) - 2\tau_0 \tan(\pi/4 + \phi/2). \tag{5}$$

The criterion for crazing can be written for the plane stress case as

$$\sigma_1 - \nu\sigma_2 = \frac{X}{\sigma_1 + \sigma_2} + Y, \tag{6}$$

where X and Y are equal to 1420 and 24.9 MN m^{-2} for a craze to form in 10 sec, and Poisson's ratio, $\nu = 0.35$. The failure criterion is shown in Fig. 1. It should be noted that the tensile strength of polystyrene is roughly ten times of that of concrete. The centred-fan slip-line field for the yield criterion of Equation 5 has been described previously [4] and is shown in Fig. 2b. There are two conditions that allow the simultaneous prediction of the indentation pressure and the extent of the fan angle, γ; these are that the total force component, F_x, acting on the boundary CEA (in Fig. 2b) should be zero, and that the tensile stress component, σ_{xx}, along EA (in Fig. 2b) should satisfy Equation 6. When the

calculation is made it is found that both the indentation pressure at $490\,MN\,m^{-2}$ and the fan angle, $\gamma = 100°$ are much larger than those found experimentally ($273\,MN\,m^{-2}$ and 60°), if the tensile stress σ_{xx} is to have a value of $60\,MN\,m^{-2}$ along the whole of EA (in Fig. 2b). In fact the indentation pressure is so large that alternative slip-line fields of the Prandtl type, with the material flowing out to both sides of the indentor, would provide lower indentation pressures. Therefore, the approach of Izbicki is inapplicable for a relatively strong brittle material like polystyrene. However, slip-line field theory can be used for *part* of the fracture process, as explained in Section 2.3.

2.2. Linear elastic fracture mechanics analysis of the growth of an existing crack

An alternative approach is to ignore yielding, assume that a crack already exists, and use a fracture mechanics analysis. Kendall [8] analysed the crack growth that may occur when a single flat indentor acts on a pre-cracked rectangular block (see Fig. 3a). He predicted the indentation force that is needed to make the crack grow, making certain assumptions about the forces that act on the top of the block, and treating the block as consisting of two cantilever beams of length equal to the crack length. It is our contention that Kendall, by neglecting the crack closure force, has derived an incorrect expression for the indentation force, F, in terms of the fracture energy, R, of the material. Secondly, it is shown, using boundary element stress analysis, that the two-beam assumption is only valid when the beams are long and slender.

In order to be consistent with the notation in Fig. 2, the indentor width is taken to be $2w$, and the block width is taken to be $2d$ (Kendall uses w and d, respectively). Kendall implicitly assumes that the indentor exerts a uniform pressure on the contact surface, so that the net force of $F/2$ acts a distance $w/2$ away from the crack. This assumption may not be valid, but should not introduce large errors if $w \ll d$. The net force produces a bending moment of $-F(d-w)/4$ about a z-axis in the neutral surface of the beam, and a compressive stress field that acts along the length of the beam. This latter stress field has no effect on the energetics of crack propagation and so may be neglected. However, the effect of a constant applied bending moment, M_Z, would be to cause the beam to deform, as is shown in Fig. 3b. In reality this cannot happen because the crack faces cannot overlap and Kendall draws the situation as in Fig. 3a with the beams touching under the indentor. Consequently, a force, G, acting horizontally, must act at $y = 0$ at the top of the beams, due to crack closure (see Fig. 3c). It is also possible, with wide indentors ($w > d/2$), that the indentor exerts a significant moment on the top surface of the beam in order to keep it horizontal. This extra moment will be neglected for narrow indentors, so that the bending moment in the left-hand beam varies according to

$$M_Z = Gy - F(d-w)/4; \quad \text{for } c > y > 0, \quad (7)$$

where the statically indeterminate force, G, can be found using Castigliano's theorem, since the horizontal deflection, δ, at the point-of-action of G is zero:

$$\delta = \frac{\partial}{\partial G}\left(\int_0^c \frac{M^2}{2EI}\,dy\right) = 0, \quad (8)$$

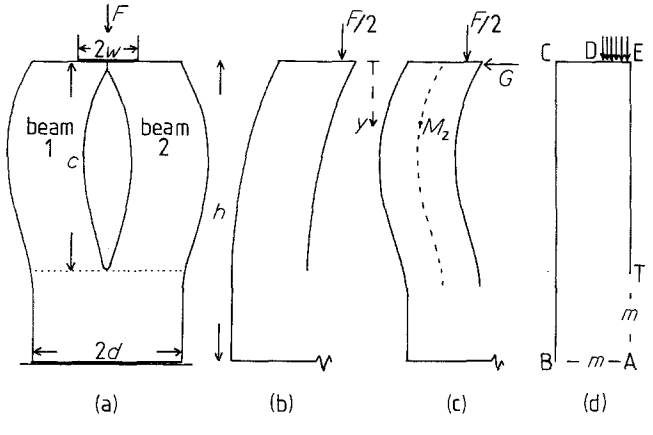

Figure 3 The specimen geometry used by Kendall. A single indentor exerts a total force, F, on the top of a rectangular precracked block. (a) shows the two-beam approximation; (b) shows the forces acting on Beam 1, according to Kendall; (c) shows the extra force, G, that acts to prevent crack closure (the bending moment at the indicated point is given by Equation 7) and (d) shows the boundary elements used, with the vectors representing the normal and shear-stress boundary conditions (the crack faces along ET cannot overlap). The crack shape in (a) is that calculated using the boundary element method for $h = 4d$, with the crack opening exaggerated 20 times so, in fact, geometrical shape changes do not affect the validity of Equation 7.

where $I = bd^3/12$ and c is the crack-length defined in Fig. 2. When Equation 7 is substituted in Equation 8 and the integral evaluated, it is found that

$$G = \frac{3(d-w)}{8c}F. \quad (9)$$

Consequently, the stored elastic energy, U, in the beam due to bending is

$$U = \int_0^c \frac{M^2}{2EI}dy = \frac{F^2(d-w)^2c}{128\,EI}. \quad (10)$$

Equation 10 shows that U is a quarter of the value calculated by Kendall, neglecting the closure-force, G. Griffith's crack-growth criterion, that the free energy of the system must decrease for crack growth to be possible, is then applied. Since the potential energy loss of the constant load, F, is twice the stored elastic energy gain of the beams, we obtained for R (often called the critical strain energy release rate G_C)

$$R = \frac{3F^2(d-w)^2}{16Eb^2d^3}. \quad (11)$$

Since neither the crack-length, c, or the block height, h, occur in Equation 11, and since, for most materials, the crack speed is an increasing function of R, the crack should propagate steadily, regardless of the h/d ratio of the block. Equation 11 can be rewritten in terms of the stress-intensity factor, K_I, at the crack tip, and the average compressive stress at the base of the block, σ_c, using, respectively,

$$ER = K_I^2(1-\nu^2), \quad (12)$$

which holds under plane-strain conditions, and

$$\sigma_c = F/(2bd) \quad (13)$$

giving

$$K_I = \sigma_c d^{1/2}\left(1-\frac{w}{d}\right)\left(\frac{0.75}{1-\nu^2}\right)^{1/2}. \quad (14)$$

Kendall, in his experiments, used polystyrene and polymethylmethacrylate specimens with a ratio $h/d = 20$, and found that, whereas cracks longer than 4 mm moved at a constant speed (d = 1.5 mm), 2 mm long cracks were reluctant to move. Our diametral compression experiments are roughly equivalent to indenting a block with $h/d = 1$ using a single indentor. It is not clear whether the two-beam approximation that leads to Equation 14 is still valid for such a squat specimen. In order to investigate this, a boundary element stress analysis [9] was made for values of h/d between 1 and 8. The conditions imposed on each segment of the boundary (see Fig. 3d) were: AB shear stress = 0, displacement in y-direction = 0; BC, CD, ET shear stress = 0, normal stress = 0; DE shear stress = 0, normal stress = $-p$. Approximately 50 boundary elements, for which the displacement discontinuity on crossing them varies linearly with position, were placed along BCDET (in Fig. 3d), and then mirror symmetry planes AB and AE were used to create further image discontinuities, that cause the boundary conditions on AB to be satisfied. Each boundary element has two disposable parameters, the shear and normal displacement discontinuity at its mid-point, and the average shear stress and normal stress on each element boundary has a specified value. The influence coefficients of each element on each segment of boundary are evaluated and the resulting set of simultaneous linear equations were solved by the Gauss–Seidel iterative method. After each iteration any negative values for the normal displacement discontinuity of elements along ET was replaced by zero to prevent crack-face overlap occurring. The normal displacement of a special crack-tip element at T allows the evaluation of K_I, and the problem can be solved for a range of crack lengths, c, to give the results shown in Fig. 4. For squat specimens with $h/d < 8$, and for short cracks with $c/d < 4$, K_I is a sharply rising function of the crack length, c. $K_I = 0$ for cracks shorter than $0.4\,d$, since such cracks remain closed.

The results in Fig. 4 can be interpreted in two ways. Firstly, they indicate the conditions under which Kendall's experiment should give steady crack growth. So long as $h > 8d$ and $c > 4d$ the computed value of K_I is within 4% of that calculated from Equation 14. Secondly, they indicate that this purely elastic theory cannot explain the splitting that occurs when crack-free square (or cylindrical) blocks, having $h = d$, are compressed. Even if short surface cracks exist, the analysis shows that such cracks remain closed. We use Equations 11 and 12 to make a rough estimate for the indentation force F/b required to fracture a cracked polystyrene block of half-width d = 14 mm, using a narrow indentor having $w \ll d$. Substituting $\nu = 0.4$ and $K = 1.0\ \mathrm{MN\,m^{-1.5}}$ we find that $F/b = 2.5\ \mathrm{MN\,m^{-1}}$, which is an order of

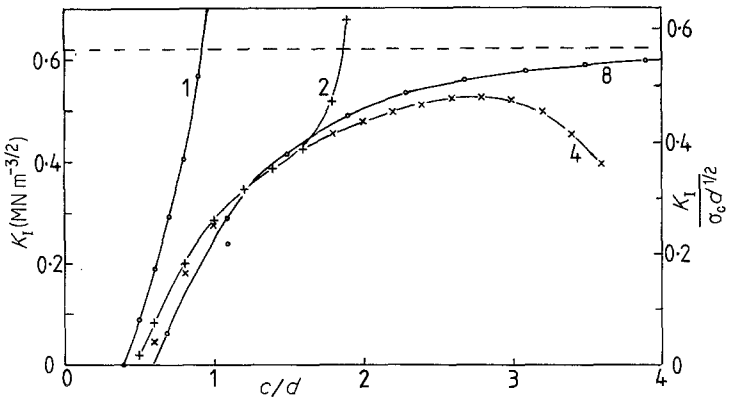

Figure 4 Predicted variation of the stress intensity factor, K_I, with the crack-length, c, in Kendall's experiment, using the boundary element method. Curves are shown for 4 block height/beam width, h/d, ratios. K is calculated for the values $\sigma_c = 20$ MN m^{-2}, $w = 0.4\,d$ and $d = 3$ mm. The right-hand scale is normalized and the dashed line shows the prediction of Equation 14.

magnitude larger than the experimental value of 0.19 MN m^{-1} for a polystyrene cylinder. Consequently, we must proceed to an elastic–plastic analysis and invoke the wedging-open action of the yielded zone to explain the indentation fracture loads for polystyrene.

2.3. An elastic–plastic fracture mechanics analysis

In this section we combine elements of the previous two sections, namely part of a slip-line field solution for a yielded zone, with a fracture mechanics analysis of crack growth. In [4] the use of an incomplete slip-line field, such as that shown in Fig. 2b with the crack only extending from E to F, was justified. According to slip-line field theory, no flow can occur since the boundary CEF is surrounded by rigid material. However, polystyrene has a low elastic modulus, and a small amount of flow occurs in the shear band pattern that is similar in shape to CED. It was shown that the boundary stresses on CED, calculated from the experimental indentation pressure and the yield criterion, were consistent with an elastic stress field outside CED that did not violate the yield criterion. This self-consistency justifies the use of the equivalent to the Henky equations for a partially developed slip-line field. It now remains to extend this approach to the analysis of crack growth.

It was observed experimentally that the yielded zone ceased to grow once the crack along EF has formed, and that the indentation force remains constant. However, it is impossible to tell whether the yield criterion is still met along the boundary CED once the crack is present, or whether it is only met within a smaller region inside CED. For the purposes of the boundary-element stress analysis it was assumed that the boundary CED remains on the point of yielding. Boundary elements were arranged along the boundary BCEF of Fig. 2b, the full specimen being created by the mirror symmetry planes AB and AF. The stress intensity factor, K_I, is calculated directly from the opening displacement of a crack-tip element at F. This avoids any necessity to calculate the stored elastic energy of the elastic region with boundary ABCEA. In an elastic–plastic problem of this kind it is not clear that R can be calculated from the energy inputs to the cylinder, because of the unknown amount of plastic work performed inside CDE as the crack grows.

It is not possible to present the results of the calculations in such a general way as for Kendall's purely elastic specimen. A particular indentation pressure was measured that caused the fracture of a polystyrene cylinder of a certain diameter, and the slip-line field extent was estimated by examining sections of the fractured cylinder. The ratio of the indentor width of 0.7 mm to the cylinder diameter of 28 mm is small at 1:40, and it was found that when larger diameter cylinders were tested, using the same indentor width, the crack initiated at the same indentation pressure. Fig. 5 shows the predicted variation of K_I with the crack length, c, for constant indentor width and indentation pressure, and for a variety of cylinder diameters. Two main conclusions can be drawn from the results.

(a) The variation of K_I with crack length is much less marked than is the case for the purely elastic analysis in Fig. 4 for $h/d = 1.0$. This can be explained simply as follows. The boundary stresses on the yielded zone for the case examined can be resolved in the x-direction to give a total splitting force, F_x, of 76.3 kN per metre thickness. The stress intensity factor for a pair of splitting forces, F, acting at the centre of a central crack in an

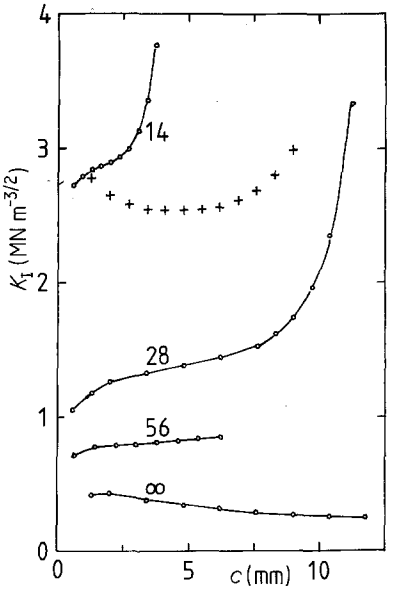

Figure 5 Predicted variation of K_I with the crack length, c, for the diametral compression of cylinders of various diameters (D in mm by curves) with indentors of $2w = 0.7$ mm and the yielded zone geometry of Fig. 2b with $\gamma = 60°$ and indentation pressure = 273 MN m^{-2}. The crosses are the prediction for $D = 28$ mm when the yielded zone boundary has failed.

infinite sheet of thickness, t, is given by

$$K_I = \frac{F}{t}(\pi c)^{-1/2}. \quad (15)$$

Hence, for very large cylinders and very long cracks, we expect K_I in the indentation case to decrease as $c^{-1/2}$. This is found to be approximately the case for the calculation of the indentation of a half space, as shown in Fig. 5. For finite cylinders the central ligament, AE, decreases in length as the crack grows yet it must still transmit the force, F_x. Consequently, the value of K_I rises as the crack-length approaches $D/2$.

As the value of K_I is approximately constant, and since for polystyrene the crack velocity is a monotonically increasing function of K_I [10] for K_I values below a critical value, this implies that when the indentation pressure is constant the crack should grow steadily. Moreover, as short cracks have nearly the same K_I values for as long cracks, the initial stages of growth of short cracks should not be difficult.

(b) As the diameter of the cylinder increases, the value of K_I decreases, and its variation with crack-length changes from always being positive, to having a maximum, and then decreasing. Hence, crack growth from a constant-width indentor should become stable, or even arrest as tests are made on larger cylinders.

Next, the effect on crack propagation of the yielded-zone boundary failing is examined. Such a failure occurs in the tests on polystyrene, and is analysed by assuming that the boundary CED (see Fig. 2b) becomes frictionless and so transmits zero shear stress. The exact normal force transmission across the boundary CE us unknown. It is approximated by assuming that $\sigma_{yy} = -p$ for $x < w$ and $\sigma_{yy} = 0$ for $x > w$ and that the other stress components are zero within the wedge CED. Consideration of the static equilibrium of the forces acting on the frictionless boundary CE shows that the normal force component is $-p$ so long as $x \leqslant 0.35$. The indentation pressure, p, is 273 MN m^{-2} for the yielded zone of extent $\gamma = 60°$. Fig.5 shows that for a 0.7 mm wide indentor on a 28 mm diameter cylinder, and for a crack length in the range 2 to 8 mm, the effect of both sides of the yielded-zone boundary failing is to make K_I jump from approximately 1.4 MN m$^{-3/2}$ to approximately 2.6 MN m$^{-3/2}$. Even if only one side of the boundary failed there would still be a significant sudden increase in the K_I value.

3. Experimental procedure

3.1. Material and specimen preparation

The polystyrene used was Shell "Carinex HR", a heat-resisting grade that, unlike general purpose polystyrene, does not contain mineral oil. The viscosity average molecular weight was 230 000, and the glass transition temperature, measured with a Perkin–Elmer differential scanning calorimeter, was 105° C. The granules were washed with methanol and dried. then compression moulded at 170° C. A number of moulds were used to give cylindrical and sheet specimens. Most of the cylinders were made with a 28 mm diameter Beckman die for preparing infra-red discs. The polystyrene was kept at 170° C under a pressure of 2 MN m^{-2} for 1 h, before slowly cooling. The 14 mm thick cylinders were then annealed at 92° C for 24 h in order to promote inhomogeneous yielding in subsequent tests. This treatment was found to give a maximum endothermic peak prior to the glass transition in DSC traces [11] indicating that the polystyrene had been fully "aged".

3.2. Compression testing

Most of the compression tests were made using

opposed flat indentors of widths in the range 0.7 to 5 mm, either acting on the diameter of a cylinder, or compressing a rectangular block. A model TTDM Instron testing maching was used with a constant cross-head speed usually of 1 mm min^{-1} at room temperature (18 to 22° C) and the specimen could be photographed during the test using, if necessary, circularly polarized monochromatic light from a sodium vapour lamp. The indentor length was usually much greater than its width (20 : 1 in some tests) so that the plane-strain deformation conditions prevailed, with negligible plastic bulging in the direction of the length of the indentors. The coefficient of friction between the polished steel indentor which has been sprayed with a fluorocarbon spray, and the polystyrene should be low. Metal-working theory [12] for the plane-strain indentation of a sheet of material of thickness $2h$ (or a cylinder of diameter $2h$) by an indentor of width $2w$ has shown that the pattern of plastic deformation depends on h/w. Therefore, some preliminary experiments were used to find the range of behaviour that occurs as h/w is varied for polystyrene.

When a cylinder is in contact with an indentor that is wider than the contact width, the situation is the same as for contact with two parallel planes. Cracks were observed to initiate at the edges of the contact width, from the flat-end surfaces of the cylinder, exactly as described by Hooper [13] for glass cylinders. When these cracks reached a certain critical size the polystyrene cylinders shattered violently. When the indentor width is equal to the contact width then shear bands initiate at the corners of the indentor, and grow in the way described previously [4]. It is only possible to achieve large plastic strains without cracks initiating if a sheet of polystyrene for which $h \leqslant 2w$ is tested. For sheets with half thicknesses, h, of $4w$ or $6w$, when a crack forms below the yielded zone, rapid fracture ensues, the crack propagating both away from the indentor and around the yielded-zone boundary. It is only when the yielded zone is small compared with h that stable crack growth becomes possible.

The sequence of events in stable crack growth, most often observed when a 28 mm diameter cylinder was indented with a 0.69 mm wide indentor at 1 mm min^{-1}, was established as follows. During photoelastic observation (see Section 3.3) the crack was observed to grow at 0.15 ± 0.03 mm sec^{-1} for between 1 and 10 mm, whereupon the crack suddenly accelerated and rapid fracture ensued. Fig. 6a shows that on the final fracture surface there is a mirror-like initial region, followed by a fast fracture region that is striated at 0.25 mm intervals. This appearance is similar to that of single-edge notch specimens examined by Friedrich [14]. Sometimes there are 2 or 3 terraces in the mirror-like region, the reasons for this being that corner cracks tend to form at the edges of the specimen (see Fig. 6b); when these link up with a centrally initiated crack that forms later these cracks are on slightly different levels. Occasionally the sudden "pop-in" that occurs when the corner cracks link across the specimen is enough of a disturbance to make the crack propagate rapidly for several mm. When the mirror-like region is examined in the SEM the fracture parabolas and brush-marks described by Doyle *et al.* [15] in their Fig. 3, are observed. If the test is stopped at this stage and a section, cut so that the crack is at the section mid-plane, is viewed from a direction normal to the crack using reflected light, the typical parallel fringe interferences pattern of a single craze is seen (Fig. 5 of Doyle [16]). Therefore, at this stage the crack is propagating with a single craze at its tip, and the crack is growing through the mid-plane of the craze. When a section is taken in a plane normal to the indentor length it is found that the yield zone boundary is intact, and that the yielded zone has wedged the crack open in the unloaded section (see Fig. 7). In order to find the sequence of events in the fast fracture process, blocks of polystyrene of size 50 mm x 50 mm x 13 mm were indented with a single 0.69 mm wide indentor. For this geometry the main crack arrests before reaching the far side of the specimen. It was found, that a new crack (or cracks), initiated at one (or both) of the indentor corners and propagated through the shear band around the boundary of the yielded zone producing a fracture surface of the type described by Friedrich [17].

When this crack joins the existing crack the specimen loading changes to that of a wedged-open edge crack. The analysis of Section 2.4 indicates that K_I would rise suddenly, and the result is seen on the fracture surface (see Fig. 8). The craze at the crack tip has suddenly failed at the craze–bulk polystyrene boundary in a way similar to that described by Doyle *et al.* [15], and fast fracture has ensued, leaving a striated fracture surface. The surface of the transition region is flatter

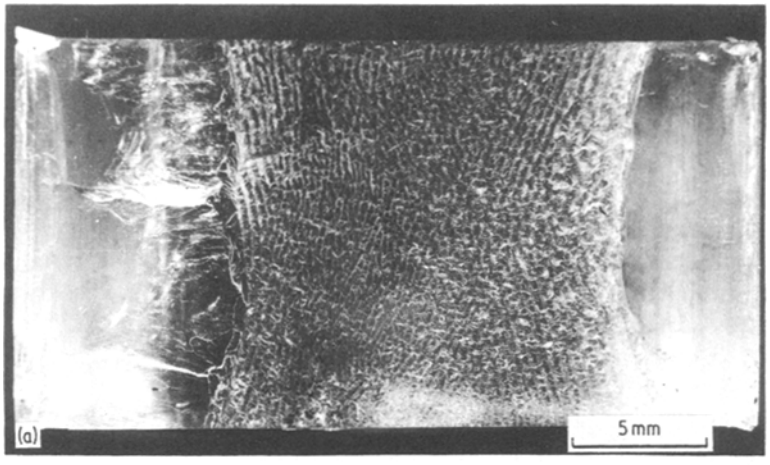

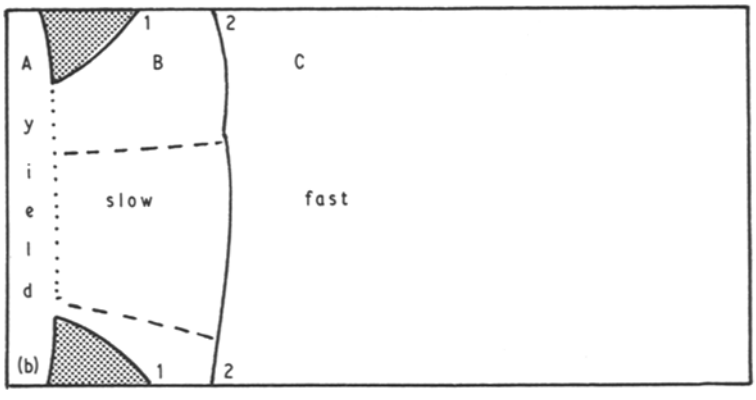

Figure 6 (a) Fracture surface of 28 mm diameter polystyrene cylinder. A is the fracture surface of the yielded zone boundary, B is the slow crack growth region and C is the rapid crack-growth region. (b) Sketch showing how corner cracks, labelled 1, can develop into a through thickness crack, labelled 2, and leave terraces on the slow fracture surface.

than that shown in Fig. 8 of Doyle [15], which shows considerable distortion of the craze material into flakes and a tree-bark pattern. Therefore, in the cylinder compression experiment a steady crack velocity has suddenly increased to a very high value as a result of the yielded-zone boundary failing. This contrasts with the single-edge notch test, which under constant load conditions is designed to give a K_I value that increases as c increases and a crack velocity that increases steadily (until an instability occurs in the crack velocity against K_I relationship [10]).

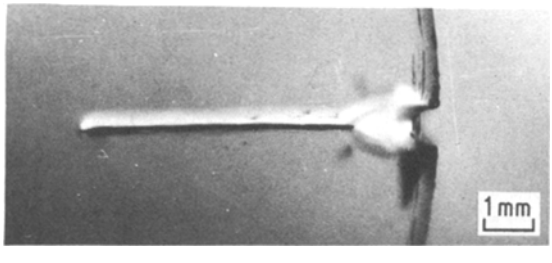

Figure 7 Transmitted-light micrograph of the yielded zone and crack in a 1 mm thick slice from a cylinder unloaded during slow crack growth.

3.3. Photoelastic observations during crack growth

First the stress optical coefficient, C, of polystyrene was established. In both the calibration experiment and the indentation experiments light of wavelength, $\lambda = 0.589\ \mu m$ travels in a direction parallel to the axis of the cylinder through a thickness, b, of polystyrene. It is assumed that the magnitude of the maximum shear stress, τ_m, does not change with the thickness co-ordinate, so that the fringe order, f, of the isochromatic fringes is related to τ_m via the relation

$$2\tau_m = Cf\lambda/b. \qquad (16)$$

In the calibration experiments the fringe order, f, was evaluated along the path AOC in Fig. A1 of the Appendix, and the contact half-width, a, was determined. Equation A3 was then used to calculate the value of τ_m, and Fig. 9 shows how f varies with τ_m for a cylinder having $b = 14.64$ mm for a range of compression forces, P, per unit thickness. (See the Appendix.) There are errors due to inaccuracies in measuring fringe positions very close to the indentor at low P values, and due to

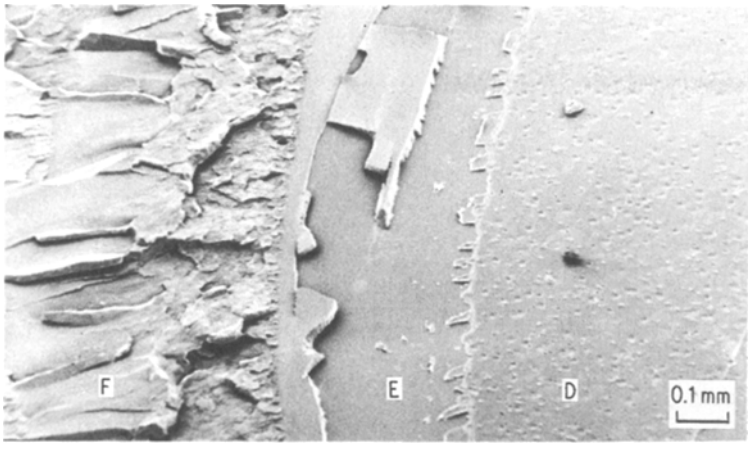

Figure 8 Scanning electron microscope photograph of the detailed appearance of the boundary between Regions B and C in Fig. 6. Region D is where the crack has grown slowly through the craze mid-plane by the coalescence of penny-shaped cracks, Region E is where the craze has suddenly failed at one of its boundaries (note a portion of craze wedge is left behind on this surface), and Region F is the fast fracture surface.

the on-set of yielding at high P values, but the best line fitted through the data gives a value of $C = 8.9 \times 10^{-12}$ m^2 N^{-1}. This is consistent with the value of 1.0×10^{-11} m^{2}N^{-1} at 20° C found for tensile tests on thin polystyrene films [18].

A series of photographs were taken during the crack growth of 28 mm diameter cylinders indented with 0.69 mm wide indentors. Fig. 10 shows the isochromatic fringe patterns towards the end of the steady crack growth regime when the crack length was 9.6 mm. It is clear that one crack is much longer than the other, and it is probable that the lower crack is only a corner crack at this stage. The fringe orders of the light fringes are indicated. Because the circular polarizing filters used give a bright background, the dark fringes occur when $f = \frac{1}{2}, 1\frac{1}{2}, 2\frac{1}{2}, \ldots$, and for $b = 12.4$ mm the corresponding values of τ_m (MN m^{-2}) are 1.3, 4.0, 6.7, 9.4, 12.1, ...

The purpose of taking the isochromatic photographs is to allow estimation of K_I at the crack tip. Usually, for single-edge notched specimens of photoelastically sensitive materials such as polycarbonate, it is possible to estimate K_I by plotting the fringe order against $r^{-1/2}$, where r is the distance from the crack tip to the maximum extent of isochromatic loop. Here there are too few isocromatic fringes and no closed loops emanating from the crack tip, so K_I has to be estimated by comparison with computed isochromatic patterns in the whole specimen. When the boundary stresses

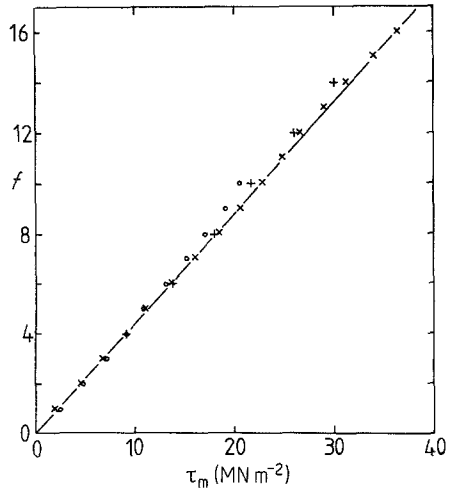

Figure 9 Photoelastic calibration of polystyrene in diametral compression, using sodium light, $\lambda = 0.589$ μm, and a light path of 14.64 mm. The isochromatic fringe number, f, is plotted against τ_{max}, calculated from the fringe position using Equation A3. ○, $P = 167$ kN m^{-1}; +, $P = 268$ kN m^{-1}; and ×, $P = 402$ kN m^{-1}.

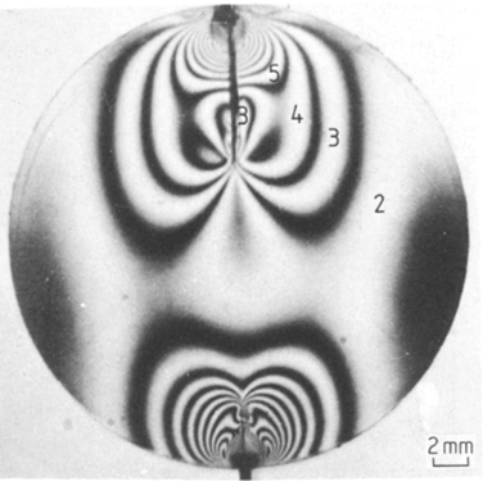

Figure 10 Isochromatic photograph of diametral compression test with the fringe number of bright fringes given. The polystyrene cylinder has diameter 28 mm, thickness 12.4 mm, and the force, F, is 2.45 kN on a 0.7 mm wide indentor.

at the slip-line field boundary for $\gamma = 60°$ were used there were significant differences between the predicted and the experimental isochromatic patterns. It was clear that, for a yielded zone plus crack length of 9.6 mm, the predicted K_I value at 1.52 MN m$^{-1.5}$ was too high. In order to find the magnitude of the error associated with the assumptions made in Section 2.3, the elastic stress field was modified empirically until it fitted the experimental isochromatic pattern. This was done by adding the effect of a pair of hypothetical forces, F'. Isochromatic patterns were calculated for a range of values of F', together with the value of K_I at the crack tip.

Fig. 11 shows the best fit of the range of predicted isochromatic patterns to the photograph in Fig. 10. As it was impossible to obtain an exact match, comparisons were made at three positions, Positions A, B and C in Fig. 11. As the extra splitting forces, F', are increased they increase the compressive stress component in their line of action at A and A′ and, hence, the isochromatic fringe order, as the stress component normal to the boundary is zero. They decrease the isochromatic fringe order at B by making the σ_{yy} stress component change from being compressive to being tensile. It was possible to match the pattern at these points by using $F' = -10$ kN m^{-1} (this compares with the total force, F_x, integrated along the yielded zone boundary of 76 kN m^{-1}) giving $K_I = 1.28$ MN m$^{-3/2}$. However, the fringe order at C is too low; this could be explained if there was some residual tensile stresses across the crack at this level, due to the crack having not penetrated to the end surfaces of the cylinder. The uncertainty in matching the isochromatic patterns means that the error in the K_I estimate is ± 0.2 MN m^{-2}. The negative F' value implies that, as the crack grows, the real yielded-zone retreats inside the boundary CED of Fig. 2b, thereby reducing F_x.

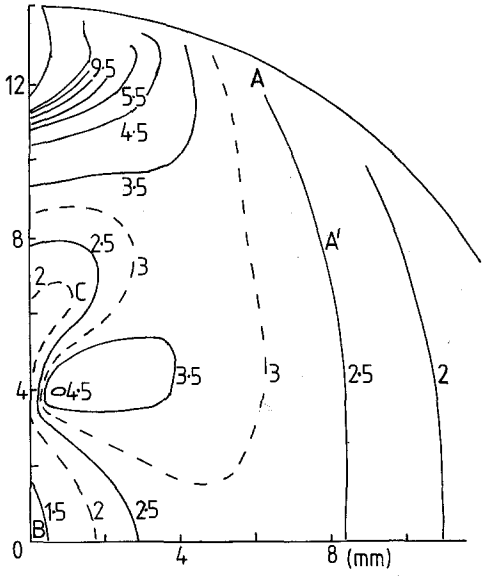

Figure 11 Isochromatic pattern predicted by the boundary element method for the experimental conditions of Fig. 10. The extra splitting forces in Fig. 3b are $F' = -10$ kN m^{-1}, and $K_I = 1.28$ MN m$^{-3/2}$ at the crack tip.

3.4. Determination of the $v(K)$ relationship for polystyrene

To find whether the stress intensity factors, K, computed or estimated from isochromatic patterns in previous sections, are sufficient to produce a crack velocity, v, of 0.15 mm sec^{-1}, it is necessary to have some independent measurements of the $v(K)$ relationship of polystyrene. Marshall *et al.* [10] have reviewed a number of earlier determinations of K_{IC} for polystyrene, and have shown how much the results are affected by the presence or absence of a craze bunch at the crack tip. They found that fatigue cracks grown at 300 Hz had a single craze at the crack tip in a general purpose grade of polystyrene of molecular weight, $M_v = 200\,000$, and the $v(K)$ relationship from cleavage and single-edge notched tests is shown in Fig. 12. It is clear from the observations of the diametral compression tests that the crack tip in those tests also had a single craze at its tip. However, since we used a heat resisting grade of a slightly higher

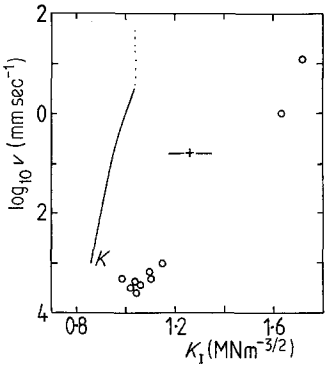

Figure 12 Log crack velocity plotted against stress intensity factor for polystyrene. The solid line is the data of [10] and K is the value deduced from [8]. The open circles represent data from double-torsion tests, and the cross represents data from the diametral compression test.

M_v value it is possible that the $v(K)$ relationship is different; consequently some double torsion crack growth experiments were undertaken. The other source of information is from Kendall's indentation experiments [8]. His polystyrene is described as Shell Carinex without a grade being specified. If his quoted fracture energy value, R, of 960 J m^{-2} at 20° C for $v = 1\ \mu$m sec^{-1} is divided by 4 to correct for error in the beam energy change analysis, and converted using Equation 12, a value of $K_I = 0.9$ MN m^{-2} is obtained, in good agreement with the values obtained by Marshall *et al.*, shown in Fig. 12.

We used the double-torsion specimen design of Evans [19], with the total specimen dimensions being 150 mm x 44 mm x 3 mm. A razor scratch was made down the centre of the specimen to prevent the crack from deviating to one side, and an initial crack 15 mm long was induced to form from a machined notch at one end, before the tests were started. The equation used to relate K_I at the crack tip, to the constant applied torque, T, on each twisted beam, the second moment of area, J, of the beam about the axis of twisting, and the material thickness, t, was

$$K_I^2 = \frac{2T^2}{Jt(1-\nu)}. \quad (17)$$

For the slower crack velocities a suspended-mass loading system was used, and the crack velocity was determined with a travelling microscope. For higher crack speeds the double-torsion specimen was tested on an Instron machine at a constant cross-head speed and at steady torque, to cause the crack growth measured. The fracture surfaces were examined both with optical and scanning electron microscopes. At the lower crack speeds of about 10^{-3} mm sec^{-1} the fracture surface is covered with the paraboli and brush-marks that were observed in the slow crack growth in the diametral compression tests. However, at crack speeds, v, of 1 mm sec^{-1} and greater it appears that multiple crazing has occurred at the crack tip. The leading edge of the crack has to grow from the razor scratch on the specimen surface, so it is not surprising that multiple crazing has occured. Consequently, in the v against K diagram of Fig. 12 the higher crack velocity points are well away from Marshall's data, whereas the low-velocity data is close. The single point from the diametral compression experiment is consistent with the other values for Carinex HR polystyrene.

3.5. Diametral compression tests on other glassy polymers

A brief survey of other materials was made to see whether the phenomena observed with polystyrene also occurred with other polymers. Polymethylmethacrylate (PMMA) would appear to have similar mechanical properties at 20° C; its compressive yield stress is similar, and the $v(K)$ relationship at low crack speeds is almost identical [10]. A 25 mm diameter rod of cast "Perspex" PMMA of high molecular weight was cut into cylinders and the ends polished with alumina paste. When these were compressed with a 0.7 mm wide indentor the maximum indentation pressure at 260 MN m^{-2} was similar to that of polystyrene. However, examination of the fractured specimen showed that the crack initiation site is quite different. Fig. 13 shows that cracks have grown from the corners of the indentors (this is Mode II or in-plane shear crack growth) and one of these cracks has propagated across the cylinder. There are no shear bands visible as PMMA at 20° C does not undergo such inhomogeneous plastic deformation. PMMA has a much higher stress for craze initiation than polystyrene; craze-size measurements at a crack-tip [20] have been interpreted to imply that the tensile stress across the crazes is 100 MN m^{-2}, that is that they are of the same order as the uniaxial yield stress. Therefore, it appears that Mode II crack growth at the indentor sides has occured before the yielded zone has become large enough, and the tensile stress at its tip has become large enough, for a craze to be initiated.

Tests were also made on polycarbonate, and a polyester thermoset (Metset SW metallurgical mounting resin). Both of these materials are far more ductile than polystyrene and, as a consequence, as the indentors moved into the plastically

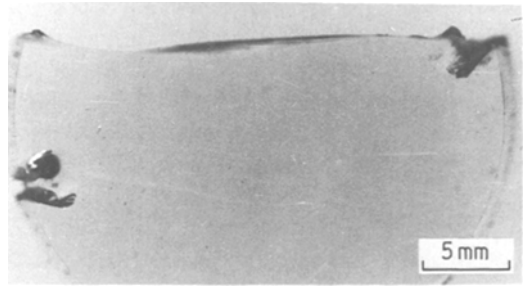

Figure 13 Crack propagation in PMMA in the diametral compression test. Cracks have formed at each corner of the indentors, and one has propagated.

deforming cylinder, a series of secondary cracks formed on the material at the side of the indentor and these cracks grew with a ductile tearing mechanism.

4. Discussion

When polystyrene cylinders are diametrally compressed the values of the fracture load are reproducible. However, it is essential to establish the sequence of events in the fracture process before calculating any of the properties of polystyrene from these fracture loads. For example, if the slip-line field analysis of Izbicki was adapted for the yield criterion of polystyrene, and the tensile strength of polystyrene calculated from this theory and the indentation pressure alone, a value of 9 MN m^{-2} would be obtained. Only observations of the yield and failure process would reveal the error; the experimental shear band pattern has a greater angular spread ($\gamma = 60°$) than the predicted 45° and, more importantly, crack growth was observed rather than instantaneous fracture. Alternatively, if the approach of Kendall was used, and the yielding under the indentor was ignored as a minor side effect, then the plane-strain fracture toughness, K_I, of polystyrene would be calculated as an extremely low value of about 0.1 MN $m^{-3/2}$. It is clear that neither of these simple approaches are fruitful.

We have established that there are two stages in the failure; in the first two types of yielding occur, and in the second three types of crack growth occur. The yielding events have been described in detail in the previous publication [4], where it is shown that the stress criterion for shear yielding determines the size of the yielded zone for any given indentation pressure, whereas the stress criterion for crazing determines the yielded zone size at which a craze initiated. The crack propagation events can be explained by combining a fracture-mechanics analysis of the, K_I, values that occur when a particular load acts on a specimen of given dimensions and given crack location and size, with measurements of the crack velocity $v(K)$ relationship for polystyrene. We have shown that a crack that initiates in the craze beneath the yielded zone below a narrow indentor has a sufficiently high and crack-length independent K_I value to allow slow stable crack growth. However, catastrophic fracture occurs after a Mode II crack propagates from the indentor edge around the yielded zone boundary. When this crack links up with the primary crack, the K_I value of the latter increases suddenly, and this causes a much higher crack velocity with a quite different crack surface morphology. It is clear then that the fracture load cannot be interpreted in terms of a single fracture strength or K_{IC} value. The cylinder diameter and indentor width also affect the results: for example while a certain indentor displacement into a small cylinder might cause complete fracture, the same displacement into a much larger cylinder would only cause a finite length of arrested crack. Nevertheless, the indentation load is roughly constant during the latter stages of the fracture process, so it is possible to say that the indentation pressure cannot exceed a certain value without fracture occurring. The fracture processes in polystyrene do not all occur with other glassy polymers; nor are they the same when polystyrene cylinders are compressed between two parallel planes. Therefore, the explanations given here are specific to polystyrene, and to the particular geometries of diametral compression tests.

In the course of searching for a suitable analysis for the polystyrene compression experiments, Kendall's theory for the splitting of precracked rectangular blocks has been reassessed. It appears that, although Kendall drew a suitable diagram of the way in which the blocks deform, he failed to include the crack closure forces in his analysis and, consequently, his formula for the fracture surface energy, R, is too large by a factor of four. In the revised analysis presented here it has still been assumed that the indentor presses with a uniform pressure on the block surface, so we have neglected any restraining moment that the indentor surface may transmit to the block by virtue of keeping part of its top surface horizontal. Therefore, any R values calculated by Kendall or the revised analysis should be treated with caution. K_I values calculated by the revised analysis from Kendall's results are within the range of K_I values published for polystyrene and PMMA, but careful experimental analysis of the loading conditions is necessary before placing much confidence in the values.

Karihaloo [21] has published a modified version of Kendall's analysis. In order to explain why the R value is not independent of the crack length he has included a frictional restraining force, αF, at the indentor interface that acts to prevent the ends of the "beams" moving apart. It is our contention that the main compressive force acts to move the

beam ends together, but that such motion is prevented by the crack closure. Karihaloo provides no experimental evidence that the crack ends do move apart, and he deduces a coefficient of friction, α, of less than 0.01, which seems unlikely. He also states that "the real state of stress under the platen is far more complicated than the simplifies state assumed here" . . . and he continues . . . "the simplification seems to be justified, judging by the answers it provides to the question raised by Kendall's theory". We dispute that the prediction of an unstable crack growth justifies his analysis. The more rigorous boundary element analysis presented here shows that it is the "two-beam" simplification that causes R to be independent of h and c in Equation 11 and not the neglect of a frictional term. Karihaloo also states that "R is independent of the sign of the applied force" in equations such as Equation 11. This may be true as the equation is presented, but it does not mean that reversing the sign of F in Fig. 3 will lead to the same value of R or K_I. This is clear if the double cantilever is considered, where a pair of splitting forces F act normal to the length of two "cantilever beams". The beams store as much elastic energy at a given magnitude of F whatever its sign, *provided the beams do not come into contact.* It is obvious, however, that a positive F causes the crack to open, whereas for a negative F the cracks close and the beams cannot store any bending energy. Therefore, Equation 11 is valid provided that F is a compressive force.

We conclude that compressive splitting tests are not a good way of producing reliable fracture-mechanics data for glassy polymers because of the uncertainties in the loading conditions applied. Diametral compression tests may be a reliable method for the quality control of concrete, but when they are applied to elastic–plastic materials a variety of fracture phenomena can occur. The plane-strain indentation tests described here confirm the possibility of surface cracking occurring as a result of compressive loads; the effects of spherical indentors in producing surface cracks, and the use of this technique to characterize orientation in polystyrene injection-moulding have recently been described [22].

The elastic–plastic fracture in polystyrene beneath a flat indentor has a parallel in the elastic–plastic fractures observed in notched bending tests in polycarbonate [23]. In both cases the shear band patterns observed bore a close resemblance to parts of standard slip-line fields, and it appears that slip-line field stress analysis gives a valid estimate of the tensile stress component required to initiate an internal craze. A fracture mechanics analysis of crack growth has not been carried out for the notched bending case, but the geometry becomes that of the edge-cracked bar once the yielded-zone boundary has failed. Once this happens the stress intensity factor, K, increases rapidly with the crack length, so accelerating crack growth. In this respect the case differs radically from the indentation cracking described here, where the K value is nearly independent of crack length, as shown in Fig. 5.

Acknowledgements

One of us (DK) is grateful to the Science Research Council for the support of a research studentship. We are grateful to the Computer Centre of the University of Birmingham for providing time on their ICL 1906A computer.

Appendix: Stress in an elastic cylinder compressed between two parallel planes

The photoelastic calibration of polystyrene was carried out by compressing a cylinder between parallel planes. As the contact width can be a significant fraction of the cylinder diameter a stress analysis that includes it is needed. Westergaard stress functions [24] can be used for the class of stress distributions for which $\sigma_{xx} = \sigma_{yy}$ and $\sigma_{xy} = 0$ along the x-axis. The maximum shear stress, τ_m, is related to the stress components, and to Westergaard's complex stress function, z''', by

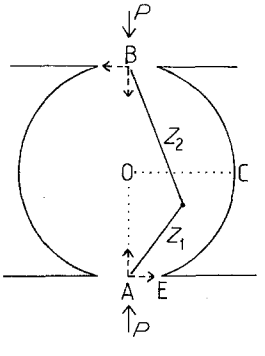

Figure A1 Co-ordinate system used in calculating the stress field in an elastic cylinder compressed between two parallel platens. The contact width is $2a$, and the maximum shear stress is calculated along the path AOC for photoelastic calibration purposes.

$$\tau_m = \tfrac{1}{2}|\sigma_{yy} - \sigma_{xx} + 2i\sigma_{xy}| = |-iyz'''|. \quad \text{(A1)}$$

For the geometry of Fig. A1, where a cylinder of diameter, D, is in contact with a rigid plane over a width, $2a$, under the action of force, P, per unit length of cylinder,

$$z''' = A|z/(a^2 - z^2)^{1/2} - i|, \quad \text{(A2)}$$

where $A = 2P/\pi a^2$. The stress field of the loading situation of Fig. A1 is built up in the same way as the line loading case [3]; stress fields due to contact at A and B are superimposed and then a uniform biaxial tension stress field of magnitude $2P/\pi D$ is superimposed. This last stress field has no effect on the maximum shear stress, so we need only consider the addition of the stress component combination $\sigma_{yy} - \sigma_{xx} + 2i\sigma_{xy}$ from the two contact stress fields. The 180° rotation between the z_1 axes with origin at A and the z_2 axes with origin at B produces no changes in this stress component combination. Consequently, addition of the two leads to

$$\pi_m = \frac{2P}{\pi a^2}\left| -\frac{iyz_1}{(a^2 - z_1)^{1/2}} - \frac{i(D-y)z_2}{(a^2 - z_2^2)^{1/2}} - D\right|, \quad \text{(A3)}$$

where $z_2 = iD - z_1$. τ_m was evaluated for 100 equally-spaced points along the path AOC in Fig. A1, for the experimentally observed contact widths.

References

1. R. P. KAMBOUR, *J. Polymer Sci. D* 7 (1973) 1.
2. P. B. BOWDEN, in "The Physics of Glassy Polymers" edited by R. N. Haward (Applied Science Publishers, London, 1973).
3. P. J. F. WRIGHT, *Mag. Concrete Res.* 7 (1955) 87.
4. D. KELLS and N. J. MILLS, *Phil Mag.* **A44** (1981) 1149.
5. R. J. IZBICKI, *Bull. Acad. Pol. Sci., Ser. des Sci. Tech.* **20** (1972) 255.
6. W. F. CHEN, "Limit Analysis and Soil Plasticity" (Elsevier, Amsterdam, New York and Oxford, 1975).
7. R. J. OXBOROUGH and P. B. BOWDEN, *Phil. Mag.* **28** (1973) 547.
8. K. KENDALL, *Proc. Roy. Soc.* **A361** (1978) 245.
9. N. J. MILLS, *J. Mater. Sci.* **16** (1981) 1317.
10. G. P. MARSHALL, L. E. CULVER and J. G. WILLIAMS, *Int. J. Fracture* 9 (1973) 295.
11. D. KELLS, PhD thesis, University of Birmingham (1979).
12. W. A. BACKOFEN, "Deformation Processing" (Addison-Wesley, Philippines, 1972) Chap. 7.
13. J. A. HOOPER, *J. Mech. Phys. Sol.* **19** (1971) 179.
14. K. FRIEDRICH, *Prakt. Metallogr.* **12** (1975) 587.
15. M. J. DOYLE, A. MARANCI, E. ORAWAN and S. T. STORK, *Proc. Roy. Soc.* **A329** (1972) 137.
16. M. J. DOYLE, *J. Mater. Sci.* **10** (1975) 159.
17. K. FRIEDRICH, *Colloid Polymer Sci.* **259** (1981) 190.
18. R. D. ANDREWS and J. F. RUDD, *J. Appl. Phys.* **28** (1957) 1091.
19. A. G. EVANS, *J. Mater. Sci.* 7 (1972) 1137.
20. E. J. KRAMER, in "Developments in Polymer Fracture" edited by E. H. Andrews (Applied Science Publishers, London, 1979) Table 1.
21. B. L. KARIHALOO, *Proc. Roy. Soc.* **A368** (1979) 483.
22. R. J. KENT, K. E. PUTTICK and J. G. RIDER, *Plast. Rubber Proc. Appl.* **1** (1981) 55.
23. N. J. MILLS, *J. Mater. Sci.* **11** (1976) 363.
24. D. S. DUGDALE and C. RUIZ, "Elasticity for Engineers" (McGraw-Hill Book Co., New York, 1971) p. 61.

Received 11 August
and accepted 30 November 1981